Research Article

대한치과재료학회지 53(1) : 1-12, 2026
Korean Journal of Dental Materials (*Korean J Dent Mater*)
ISSN:2384-4434 (Print); 2384-3268 (Online)
Available online at http://www.kadm.org
http://dx.doi.org/10.14815/kjdm.2026.53.1.1

가시광선에 의해 강화된 NiTi-O 나노튜브 및 금 나노입자 코팅된 NiTi 형상기억합금의 골형성 기능

길도건[1], 문경숙[2], 오승한[2], 최은주[1,*]

[1]원광대학교 치과대학 구강악안면외과학교실 및 원광치의학연구소
[2]원광대학교 치과대학 치과생체재료학교실 및 생체재료매식연구소

The Visible Light-Enhanced Osteogenic Functionality of NiTi-O Nanotube and Au-coated NiTi Shape Memory Metal Alloy

Do-Geon Gil[1], Kyoung-Suk Moon[2], Seung-Han Oh[2], Eun Joo Choi[1,]*

[1]Department of Oral and Maxillofacial Surgery and Wonkwang Dental Research Institute, College of Dentistry, Wonkwang University, Iksan, Republic of Korea
[2]Department of Dental Biomaterials and the institute of Biomaterials and Implants, Wonkwang University College of Dentistry, Iksan, Republic of Korea

본 연구는 양극산화된 티타늄 산화물 나노튜브(NTO), 금(Au) 코팅, 그리고 가시광선(600 nm) 조사로 표면 개질된 니켈-티타늄(NiTi) 형상기억합금 판의 골 재생 잠재력을 평가하였다. 실험군은 NiTi, NTO, Au-NiTi-O(ANT) 대조군과 광조사된 NTO/600 및 ANT/600 그룹(600 nm, 10분, 5.5 mW/cm^2) 등 총 5개 그룹으로 설정되었다. 6주령 쥐의 두개골에 8 mm 원형 결손을 형성하였으며, 수술 후 2주와 6주 시점에 마이크로 CT 및 조직학적 분석을 통해 골 재생을 평가하였다. 2주차 결과, ANT 및 ANT/600 그룹이 더 높은 신생골 부피(각각 3.381 ± 1.220 및 2.606 ± 1.721 mm^3)를 나타냈으나, 통계적으로 유의한 차이는 없었다($p > 0.05$). 6주차에는 그룹 간 유의미한 차이가 관찰되었는데, ANT 그룹이 가장 높은 골 부피를 보인 반면, NTO 그룹은 유의하게 낮은 골 형성을 나타냈다. 그러나 조사군과 비조사군을 비교했을 때, 가시광선 조사에 의한 통계적으로 유의미한 골 형성 증진 효과는 확인되지 않았다. 조직학적 소견상 모든 그룹의 NiTi 판 인접부에서 일관된 신생골 형성이 관찰되었으며, 이는 NTO 그룹의 낮은 골 부피가 소재의 세포독성이 아닌 기계적 불안정성과 판의 변위에 기인했음을 시사한다. 제한적인 광자극 효과는 비다공성 판 구조와 연조직에 의한 600 nm 빛의 감쇠 때문인 것으로 판단된다. 결론적으로, 개질된 NiTi 표면은 우수한 생체적합성을 입증하였으나, 효과적인 광활성화를 달성하기 위해서는 향후 기계적으로 안정적인 다공성 NiTi 판의 개발과 광학 변수의 최적화 연구가 필요하다.

색인단어 : NiTi 형상기억합금, 금 코팅, 플라즈모닉 광촉매, 가시광선 조사, 골 재생

Do-Geon Gil (ORCID: 0000-0002-5756-3352)
Kyung-Suk Moon (ORCID: 0000-0001-6534-3045)
Seunghan Oh (ORCID: 0000-0002-7250-721X)

*Correspondence: Eun-Joo Choi (ORCID: 0000-0002-6981-8439)
460 Iksan-daero, Iksan, Jeonbuk 54538, Republic of Korea
Affiliation: Department of Oral and Maxillofacial Surgery, College of Dentistry, Wonkwang University, Iksan, Republic of Korea
Tel: +82-63-859-2921
E-mail: cejoms@wku.ac.kr

Received: Oct. 16, 2025; Revised: Nov. 14, 2025; Accepted: Dec. 02, 2025

Introduction

To ensure mechanical stability and long-term osseointegration, adequate alveolar bone volume and height are critical prerequisites for successful dental implant placement. In cases of alveolar bone deficiency due to trauma, infection, or resorption following tooth extraction, bone augmentation procedures such as guided bone regeneration (GBR), sinus lift, or distraction osteogenesis are required before or during implant surgery. Titanium plates have been widely used as space-maintaining membranes to stabilize graft materials and prevent soft tissue collapse, thereby enabling vertical and horizontal bone augmentation (1-3). However, titanium plates frequently cause complications, such as soft tissue dehiscence, infection, and difficulty in surgical handling, owing to their rigidity and lack of shape adaptability, thereby limiting their clinical applicability to complex anatomical regions (4, 5).

To overcome these limitations, shape memory alloys (SMAs), particularly nickel-titanium (NiTi) alloys, have emerged as promising biomaterials. NiTi exhibits unique thermoelastic and superelastic properties, allowing deformation at low temperatures and spontaneous recovery of its original configuration upon heating. These characteristics allow the fabrication of self-expanding or self-stabilizing medical devices that can adapt to the surrounding tissues (6-8). In maxillofacial surgery, NiTi plates can be pre-shaped to match bone contours and then induce gradual periosteal elevation as they recover, creating an osteogenic environment through a "tenting effect" (9). Moreover, NiTi exhibits high corrosion resistance, fatigue strength, and biocompatibility, which have led to its extensive use in orthodontic wires, cardiovascular stents, and orthopedic fixation systems (10, 11).

Recent surface modification techniques have enhanced the bioactivity of NiTi-based implants. The formation of NiTi-O nanotubes (NTOs) via anodization increases surface area, wettability, and protein adsorption, thereby improving cell adhesion and osteogenic differentiation (12, 13). The introduction of noble metals such as gold (Au) or platinum (Pt) onto nanotube surfaces has been reported to provide additional functionalities, including antibacterial properties, improved hemocompatibility, and photoactivation capability through localized surface plasmon resonance (LSPR) (14-16). In particular, Au NPs possess high biostability and electrical conductivity, which may synergistically promote osteoblastic differentiation via ROS-mediated signaling or photothermal conversion under visible-light irradiation (17-19).

Visible light, particularly in the range of 550–650 nm, is recognized for its mild photothermal and photobiomodulatory effects on living tissues. Unlike ultraviolet light, which induces oxidative stress and DNA damage, visible light can activate cellular signaling pathways such as mitochondrial cytochrome c oxidase activity, ATP synthesis, and osteogenic gene expression (20-22). The photothermal activation of plasmonic nanoparticles on implant surfaces can enhance local microcirculation, induce mild thermal stimulation, and modulate osteoblast differentiation without cytotoxicity (23, 24). When integrated with NiTi shape memory alloys, this visible light-driven response may serve as a controllable, noninvasive stimulus to accelerate bone healing during the early postoperative period.

Based on these scientific rationales, we hypothesized that the incorporation of NiTi-O nanotubes and Au nanoparticles on the surface of NiTi shape memory alloys would enable visible light-induced plasmonic activation and enhance osteogenic performance. The hypothesis of this study was that localized photothermal stimulation induced by visible light irradiation enhances osteogenic signaling by inducing intracellular ROS and ATP production. In the present study, we performed an *in vivo* experiment to test this hypothesis. *In vivo* experiments were conducted using a rat calvarial defect model to

evaluate bone formation quantitatively using micro-computed tomography (micro-CT) and histological analysis. This study aimed to establish a scientific basis for visible-light-responsive activation of NiTi-based biomaterials as a next-generation strategy for bone regeneration and dental implant applications.

Materials and Methods

1. Sample Preparation

Table 1 lists all experimental groups tested in this study. Five groups were established: three control groups (NiTi, NTO, ANT) and two light-irradiated experimental groups (NTO/600, ANT/600; LED wavelength = 600 nm, irradiation time = 10 min, intensity = 5.5 mW/cm^2). NiTi-O nanotubes were fabricated via anodization of NiTi sheets (5 × 5 cm^2, 0.127 mm, Alfa Aesar, USA). Surfaces were sequentially polished with 600-, 1200-, and 2000-grit SiC papers, ultrasonically cleaned, and anodized in ethylene glycol containing 0.2 wt% NH_4F (Sigma Aldrich Co., MO, USA) and 1 vol% deionized water at 25 V for 1 h. After rinsing and drying at 60 ℃, the samples were annealed at 400 ℃ for 3 h (1 K/min) to crystallize the nanotubes. Au coatings were deposited using ion plasma sputtering (E-1030, Hitachi Co., Tokyo, Japan) for 3 s to obtain Au-NiTi-O nanotubes (ANT).

2. Animal Model and Surgical Procedure

Fifty 6-week-old male Sprague-Dawley rats (280 ± 20 g) were randomly assigned to five groups (n = 10). The animals were housed under controlled temperature and humidity with a 12-h light/dark cycle and acclimatized for one week. General anesthesia was induced using Zoletil (10 mg/kg; Bayer Korea Ltd., Seoul, Korea) and Rompun (5 mg/kg; Bayer Korea Ltd., Seoul, Korea), followed by local infiltration with 2% lidocaine containing 1:100,000 epinephrine. A midline incision was made to expose the calvarium, and an 8 mm–diameter defect was created using a trephine bur (THB80; Osung MND Co., Kimpo, Korea) without damaging the dura. Each defect was covered with a sample disc (NiTi, NTO, ANT, NTO/600, ANT/600) and then sutured using 5-0 nylon. The light-irradiated groups received 600 nm LED exposure (10 min/session) twice per week (five sessions for 2 weeks, 13 sessions for 6 weeks). The LED device was attached to the top cover of the cage (total height, 18 cm). Considering the height of the rats (approximately 13–15 cm), the distance between the light source and calvarial defect surface ranged from 3 to 5 cm during irradiation. The conditions of 600 nm LED irradiation were based on previous studies (22, 23), which reported photobiostimulation effects at the cellular level. After 2 and 6 weeks, the animals were sacrificed via CO_2 asphyxiation. The calvaria were harvested and fixed in 4% paraformaldehyde

Table 1. Experimental groups tested in this study

Surface Type	Visible Light	Group Name
NiTi	None	NiTi
NiTi-O nanotube	None	NTO
NiTi-O nanotube	600 nm LED	NTO/600
Au-coated NiTi-O nanotube	None	ANT
Au-coated NiTi-O nanotube	600 nm LED	ANT/600

for 48 h. The procedure for the *in vivo* experiments was approved by the Wonkwang University IACUC (no. WKU23-58). Figure 1 shows the creation of an 8 mm-diameter circular calvarial defect in the rat skull (left) and placement of the experimental specimen over the defect site (right).

3. Micro-CT analysis

Bone regeneration was evaluated using a high-resolution micro-CT system (SkyScan 1076; SkyScan Co., Aartselaar, Belgium). Specimens fixed in 10% neutral-buffered formalin were scanned at 100 kV, 100 μA, and an 18 μm voxel size with a 0.5 mm aluminum filter. Quantitative analysis was conducted using CTAn software (v1.20.3.0). To distinguish the mineralized bone from the background, the lower and upper threshold values were set at 55 and 95 (grayscale values), respectively. The analysis was performed within a circular region of interest (ROI, 8 mm diameter) corresponding to the defect.

4. Hematoxylin & Eosin (H&E) staining

H&E staining was performed as follows: Tissue samples were fixed in 10% neutral-buffered formalin for 24-48 h, dehydrated using graded ethanol, and embedded in paraffin. Sections of 4-5 μm thickness were prepared, deparaffinized with xylene, rehydrated, and stained with hematoxylin for 5 min. After rinsing, differentiation and bluing were performed, followed by counterstaining with eosin for 1-2 min. The slides were dehydrated, cleared, and mounted with resin. The stained sections were observed to assess new bone formation and tissue morphology.

5. Statistical analysis

Data are presented as mean ± standard deviation (SD) unless otherwise stated. Statistical analysis was performed using SPSS software (version 23.0; SPSS Inc., Chicago, IL, USA). One-way analysis of variance (ANOVA) was used to compare experimental groups. Post hoc comparisons were performed using the Games-Howell test. Statistical significance was set at $p<0.05$.

Results

1. Micro-CT analysis

Table 2 lists the bone volume values for all experimental groups calculated by micro-CT analysis within the regions of interest. The number of samples analyzed in each group ranged from 4 to 6, as detailed in Table 2. At 2 weeks, the ANT and ANT/600 groups showed higher new bone volumes(3.381 ± 1.220 and 2.606 ± 1.721 mm^3, respec-

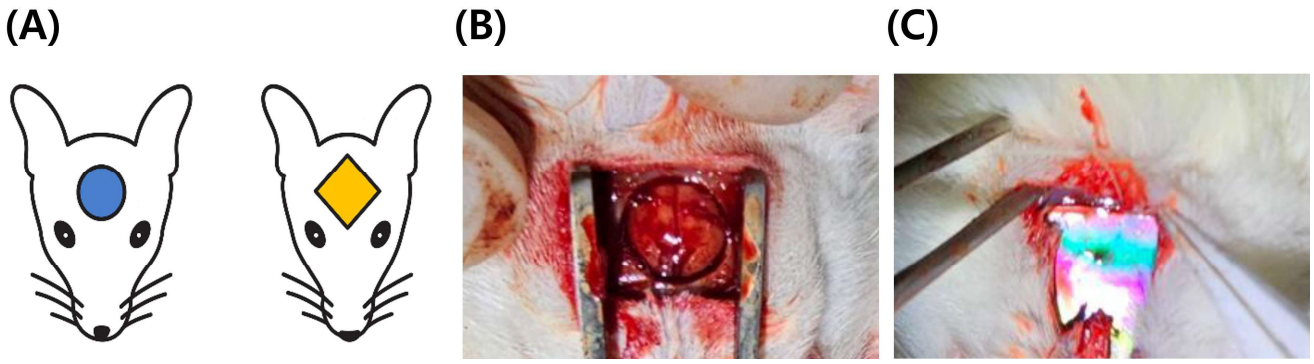

Figure 1. The illustration images (A) and photographic images of creating an 8 mm-diameter circular calvarial defect in a rat skull (B) and placing the experimental specimen over the defect site (C).

Table 2. Bone volume within the region of interest quantified by micro-computed tomography (micro-CT) at 2 and 6 weeks after surgery. Data are presented as mean ± standard deviation (SD) (unit: mm^3). The number of samples analyzed in each group is indicated

Group	2 weeks	Number of samples	6 weeks	Number of samples
	Mean (SD)		Mean (SD)	
NiTi	2.206 (1.195)^{a}	5	8.058 (3.813)^{A,B}	4
NTO	2.380 (2.299)^{a}	4	0.440 (0.269)^{B}	4
ANT	3.381 (1.220)^{a}	5	13.588 (8.628)^{A}	4
NTO/600	1.726 (0.541)^{a}	5	11.123 (2.913)^{A,B}	4
ANT/600	2.606 (1.721)^{a}	6	6.156 (2.917)^{A,B}	4

* Different lowercase letters indicate statistically significant differences among groups at 2 weeks, while different uppercase letters indicate statistically significant differences among groups at 6 weeks (p<0.05).

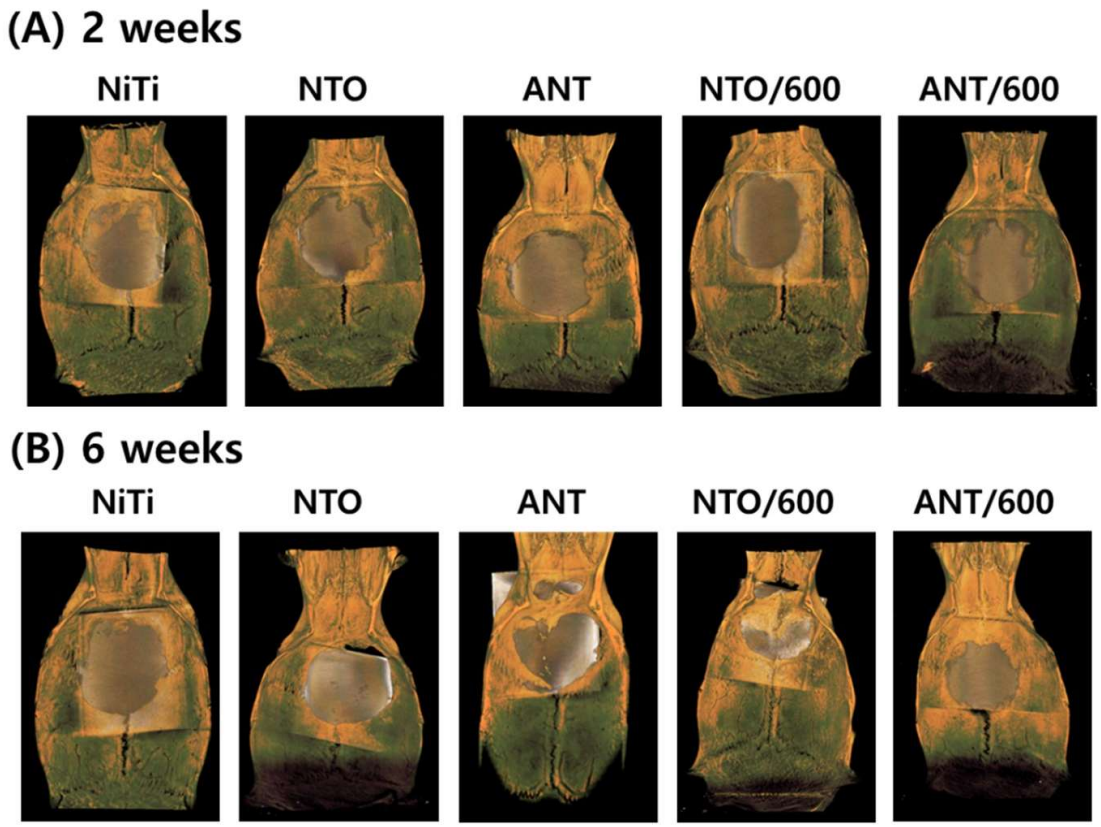

Figure 2. Representative three-dimensional micro-computed tomography (micro-CT) reconstructions of rat calvarial defects in the NiTi, NTO, and ANT groups with and without visible light irradiation at (A) 2 weeks and (B) 6 weeks post-operation. The images illustrate the spatial morphology of the calvarial defects and the extent of mineralized tissue formation within the defect region over time.

tively) compared to the other groups; however, these differences were not statistically significant (p>0.05).

At 6 weeks postoperatively, the bone volumes were 8.058 ± 3.813 mm^3 for NiTi, 0.440 ± 0.269 mm^3 for NTO, 13.588 ± 8.628 mm^3 for ANT, 11.123 ± 2.913 mm^3 for NTO/600, and 6.156 ± 2.917 mm^3 for ANT/600. Significant group- dependent differences were observed at this time point (p<0.05). Specifically, the ANT group demonstrated

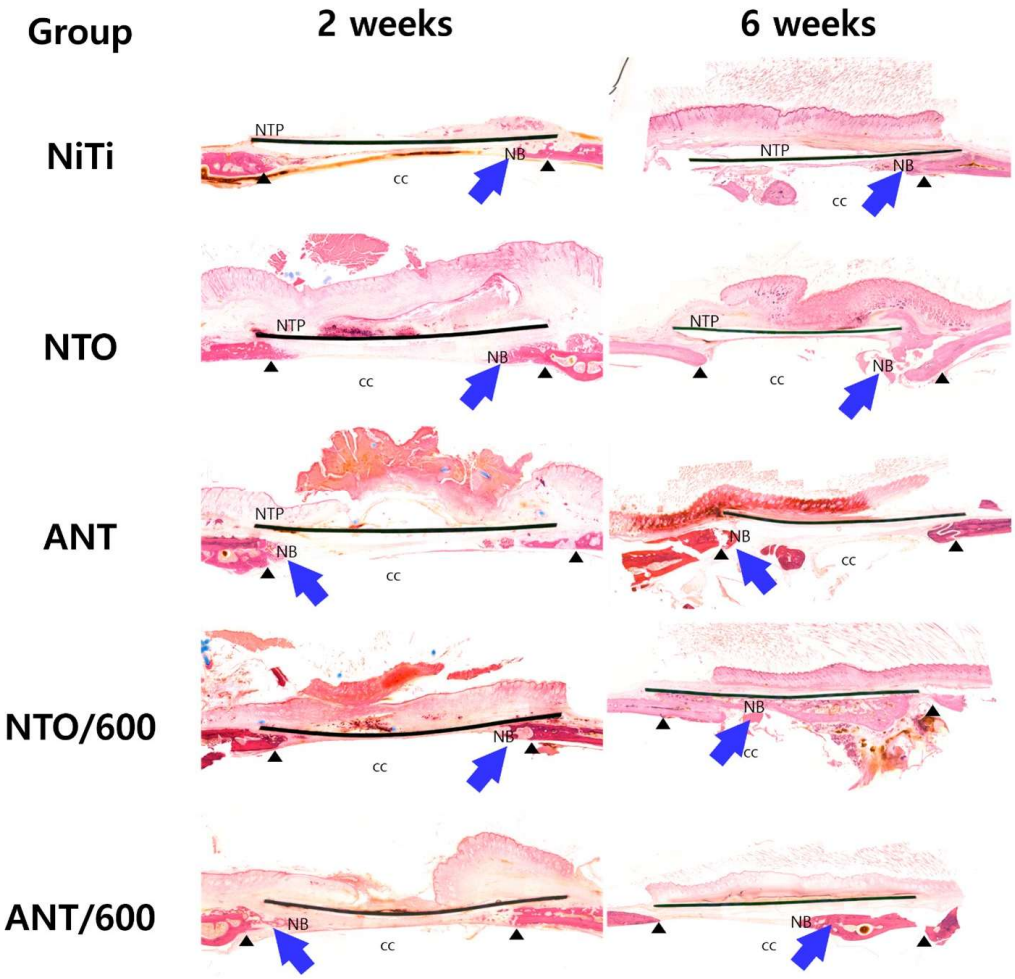

Figure 3. Representative hematoxylin and eosin (H&E)–stained histological sections of rat calvarial defects. The calvarial defect margins are indicated by black arrowheads, while newly formed bone within the defect area is indicated by blue arrows. In all specimens, new bone formation is observed adjacent to the NiTi plate (NTP), extending along the defect region over the cranial cavity (cc). (NTP: NiTi plate; NB: newly formed bone; cc: cranial cavity.)

the highest bone volume, which was significantly greater than that of the NTO group. The other groups (NiTi, NTO/600, and ANT/600) showed intermediate values with no statistically significant differences compared to either the ANT or NTO groups. In the 6-week experimental period, plate displacement from the sub-periosteal region was frequently observed, particularly in the NTO group.

Although our initial criterion was to exclude such displaced specimens to ensure data reliability, applying this strictly to the NTO group would have resulted in an excessive loss of data points, making statistical analysis impossible.

Therefore, for the NTO group, all surviving specimens were included in the volumetric analysis regardless of minor displacements. Consequently, the exceptionally low bone volume observed in the NTO group at 6 weeks should be interpreted with the understanding that mechanical instability likely compromised the osteogenic outcome.

Figure 2 shows the three-dimensional micro-computed tomography (micro-CT) reconstruction images of rat calvarial defects in the NiTi, NTO, and ANT groups, with and without visible light irradiation.

2. Hematoxylin & Eosin (H&E) staining

Figure 3 illustrates hematoxylin and eosin (H&E)–stained histological sections of rat calvarial defects. As shown in Figure 3, histology confirmed new bone formation in all groups at 2 and 6 weeks but without distinct qualitative differences in biocompatibility. In some cases, new bone was observed directly in contact with the NiTi plates, and no inflammatory cell infiltration was observed.

Discussion

This study evaluated bone regeneration in rat calvarial defects using NiTi SMAs modified with nanotubes, gold coatings, and visible light irradiation. Although the hypothesis of light-enhanced osteogenesis was not statistically supported, the data provide valuable *in vivo* insights. The use of non-porous plates, necessitated by fabrication challenges, likely restricts cellular and vascular infiltration, thereby constraining osteoconduction.

Regarding the photostimulatory effect, no statistically significant enhancement specifically attributable to LED irradiation was detected when comparing the irradiated groups (NTO/600 and ANT/600) with their non-irradiated counterparts (NTO and ANT) at 6 weeks postoperatively. The most likely explanation for this is the insufficient and non-uniform tissue dosimetry of 600 nm light in vivo. Although the 600 nm wavelength falls within the therapeutic optical window, its penetration capability is inherently limited compared to near-infrared (NIR) wavelengths owing to absorption and scattering by tissue chromophores, such as hemoglobin and melanin (25, 26). Previous studies have indicated that light intensity attenuates significantly even when light passes through thin soft tissue layers (27, 28). In this study, the rat scalp (approximately 1–3.6 mm thick) acting as a barrier likely absorbed a substantial portion of the incident photon energy, preventing the threshold localized surface plasmon resonance (LSPR) required for enhanced osteogenesis.

In terms of material comparison, significant differences in bone volume were observed between the specific groups, with the NTO group showing a significantly lower bone volume than the ANT group. This result is likely attributable to mechanical instability rather than material cytotoxicity. The lack of fixation allowed minor displacements that introduced variability and reduced the reproducibility of the micro-CT quantification. Continuous micro-movements of the non-fixed plates likely exerted physical irritation on the regenerating tissue, provoking osteoclastic activity and subsequent bone resorption (29, 30). This interpretation is supported by histological observations, which consistently showed new bone apposition adjacent to the NiTi surfaces across all groups, indicating excellent biocompatibility despite quantitative discrepancies.

Several limitations inherent to the experimental design are noted. The 8 mm critical-size calvarial model can introduce variability owing to methodological factors. Additionally, the general reduction trend or fluctuation across groups may reflect the physiological remodeling phase, in which the initially formed immature woven bone is resorbed and replaced by mature lamellar bone. Most importantly, the geometric instability caused by the absence of fixation pins is a confounding factor that likely underestimates the osteogenic potential of the materials.

Given the limitations of this study, future investigations should focus on two main strategies. To overcome optical limitations, near-infrared (NIR) sources should be considered to achieve deeper and more homogeneous energy delivery (31, 32). In addition, a new NiTi specimen design should be adopted to enhance mechanical stability after implantation. Pore-textured NiTi specimens are also expected to facilitate improved cell infiltration and vascularization. This technology holds potential for

applications in clinical bone regeneration fields, such as alveolar bone augmentation and implant site reconstruction.

Conclusion

In summary, this study demonstrated the osteogenic potential of surface-modified NiTi alloys, particularly the Au-coated NiTi-O nanotube (ANT) surface, which exhibited the highest bone volume at six weeks. The NTO group showed significantly less bone formation, which was attributed to mechanical instability and plate displacement rather than material cytotoxicity, as evidenced by the consistent histological observation of new bone apposition adjacent to the NiTi surfaces across the groups. Although visible light irradiation did not yield a statistically significant enhancement in bone volume under the current conditions compared with non-irradiated controls, the overall findings validate the fundamental biocompatibility of the material. The limited photostimulatory effect was likely attributable to geometric and optical constraints, such as the nonporous plate design and light attenuation by the soft tissue. Therefore, future studies should focus on developing mechanically stable porous NiTi mesh structures and optimizing the optical parameters to fully leverage the synergistic potential of photothermal activation on this highly biocompatible platform.

Acknowledgments

This research was supported by the National Research Foundation of Korea (NRF), grant number 2021R1A2C 1004283, funded by the Korean government (MSIT). Also, this study includes partial content extracted from the master's thesis of Do-Geon Gil.

References

1. Rakhmatia YD, Ayukawa Y, Furuhashi A, Koyano K. Current barrier membranes: Titanium mesh and other membranes for guided bone regeneration in dental applications. J Prostho Res. 2013;57(1):3-14.
2. Xie Y, Li S, Zhang T, Wang C, Cai X. Titanium mesh for bone augmentation in oral implantology: current application and progress. Int J Oral Sci. 2020;12(1):37.
3. Shi Y, Liu J, Du M, Zhang S, Liu Y, Yang H, et al. Customized Barrier Membrane (Titanium Alloy, Poly Ether-Ether Ketone and Unsintered Hydroxyapatite/ Poly-l-Lactide) for Guided Bone Regeneration. Front Bioeng Biotechnol. 2022;10:916967.
4. Poli PP, Beretta M, Cicciu M, Maiorana C. Alveolar ridge augmentation with titanium mesh. A retrospective clinical study. Open Dent J. 2014;8:148-58.
5. Zhu S, Chen Y, Lin F, Chen Z, Jiang X, Zhang J, et al. Complications following titanium cranioplasty compared with nontitanium implants cranioplasty: A systematic review and meta-analysis. J Clin Neurosci. 2021;84:66-74.
6. Samal S, Tomáštík J, Václavek L, Chandra M, Kopeček J, Stachiv I, et al. Recovery of deformation surface of superelastic and shape memory NiTi alloy. Appl Surf Sci Adv. 2025;25:100684.
7. Yamauchi K, Nogami S, Martinez-de la Cruz G, Hirayama B, Shimizu Y, Kumamoto H, et al. Timedrelease system for periosteal expansion osteogenesis using NiTi mesh and absorbable material in the rabbit calvaria. J Cranio Maxill Surg. 2016;44(9): 1366-72.
8. Kapoor D. Nitinol for Medical Applications: A Brief Introduction to the Properties and Processing of Nickel Titanium Shape Memory Alloys and their Use in Stents Considerations for the manufacture of Nitinol parts for stents and some other medical applications. Johnson Matthey Tech. 2017;61(1):66-76.

9. Yamauchi K, Nogami S, Tanaka K, Yokota S, Shimizu Y, Kanetaka H, et al. The Effect of Decortication for Periosteal Expansion Osteogenesis Using Shape Memory Alloy Mesh Device. Clin Implant Dent Relat Res. 2015;17:E376-E84.
10. Ryhänen J. Biocompatibility of Nitinol. Minim Invasiv Ther. 2000;9(2):99-105.
11. Kujala S, Pajala A, Kallioinen M, Pramila A, Tuukkanen J, Ryhänen J. Biocompatibility and strength properties of nitinol shape memory alloy suture in rabbit tendon. Biomaterials. 2004;25(2):353-8.
12. Hang R, Liu Y, Zhao L, Gao A, Bai L, Huang X, et al. Fabrication of Ni-Ti-O nanotube arrays by anodization of NiTi alloy and their potential applications. Sci Rep. 2014;4(1):7547.
13. Hang R, Zhao F, Yao X, Tang B, Chu PK. Selfassembled anodization of NiTi alloys for biomedical applications. Appl Surf Sci. 2020;517:146118.
14. Sun Y, Xu W, Jiang C, Zhou T, Wang Q, A L. Gold nanoparticle decoration potentiate the antibacterial enhancement of TiO(2) nanotubes via sonodynamic therapy against peri-implant infections. Front Bioeng Biotechnol. 2022;10:1074083.
15. Qin LP, Wang GJ, Tan YW. Plasmonic Pt nanoparticlesTiO hierarchical nano-architecture as a visible light photocatalyst for water splitting. Sci Rep. 2018;8(1): 16198
16. Dong F, Wang HQ, Sen G, Wu ZB, Lee SC. Enhanced visible light photocatalytic activity of novel Pt/C-doped TiO2/PtCl4 three-component nanojunction system for degradation of toluene in air. J Hazard Mater. 2011;187 (1-3):509-16.
17. Zhang D, Liu D, Zhang J, Fong C, Yang M. Gold nanoparticles stimulate differentiation and mineralization of primary osteoblasts through the ERK/MAPK signaling pathway. Mater Sci Eng C Mater Biol Appl. 2014;42:70-7.
18. Rau LR, Huang WY, Liaw JW, Tsai SW. Photothermal effects of laser-activated surface plasmonic gold nanoparticles on the apoptosis and osteogenesis of osteoblast-like cells. Int J Nanomedicine. 2016;11: 3461-73.
19. Yi C, Liu D, Fong C-C, Zhang J, Yang M. Gold Nanoparticles Promote Osteogenic Differentiation of Mesenchymal Stem Cells through p38 MAPK Pathway. ACS Nano. 2010;4(11):6439-48.
20. Zheng J, Zhang X, Zhang Y, Yuan F. Osteoblast differentiation of bone marrow stromal cells by femtosecond laser bone ablation. Biomed Opt Express. 2020;11(2):885-94.
21. Wei M, He X, Liu N, Deng H. Role of reactive oxygen species in ultraviolet-induced photodamage of the skin. Cell Div. 2024;19(1):1.
22. Da Silva D, Crous A, Abrahamse H. Enhancing osteogenic differentiation in adipose-derived mesenchymal stem cells with Near Infra-Red and Green Photobiomodulation. Regen Ther. 2023;24:602-16.
23. Li L, Wu J, Liu L, Zhang P, Zhang Y, Zhou Z, et al. Photothermal Antibacterial Effect of Gold Nanostars Coating on Titanium Implant and Its Osteogenic Performance. Int J Nanomedicine. 2025;20:5983-99.
24. Zhou R, Zhang M, Xi J, Li J, Ma R, Ren L, et al. Gold Nanorods-Based Photothermal Therapy: Interactions Between Biostructure, Nanomaterial, and Near-Infrared Irradiation. Nanoscale Res Lett. 2022;17(1):68.
25. Ash C, Dubec M, Donne K, Bashford T. Effect of wavelength and beam width on penetration in lighttissue interaction using computational methods. Lasers Med Sci. 2017;32(8):1909-18.
26. Jacques SL. Optical properties of biological tissues: a review. Phys Med Biol. 2013;58(11):R37-61.
27. Chung H, Dai T, Sharma SK, Huang YY, Carroll JD, Hamblin MR. The nuts and bolts of low-level laser (light) therapy. Ann Biomed Eng. 2012;40(2):516-33.
28. Bashkatov AN, Genina EA, Kochubey VI, Tuchin VV. Optical properties of human skin, subcutaneous and

mucous tissues in the wavelength range from 400 to 2000 nm. J Phys D Appl Phys. 2005;38(15):2543-55.
29. Szmukler-Moncler S, Salama H, Reingewirtz Y, Dubruille JH. Timing of loading and effect of micromotion on bone-dental implant interface: review of experimental literature. J Biomed Mater Res. 1998; 43(2):192-203.
30. Duyck J, Vandamme K, Geris L, Van Oosterwyck H, De Cooman M, Vandersloten J, et al. The influence of micro-motion on the tissue differentiation around immediately loaded cylindrical turned titanium implants. Arch Oral Biol. 2006;51(1):1-9.
31. Tsai SR, Hamblin MR. Biological effects and medical applications of infrared radiation. J Photochem Photobiol B. 2017;170:197-207.
32. Sordillo LA, Pu Y, Pratavieira S, Budansky Y, Alfano RR. Deep optical imaging of tissue using the second and third near-infrared spectral windows. J Biomed Opt. 2014;19(5):056004.

Research Article

The Visible Light-Enhanced Osteogenic Functionality of NiTi-O Nanotube and Au-coated NiTi Shape Memory Metal Alloy

Do-Geon Gil[1], Kyoung-Suk Moon[2], Seung-Han Oh[2], Eun Joo Choi[1,]*

[1]*Department of Oral and Maxillofacial Surgery and Wonkwang Dental Research Institute, College of Dentistry, Wonkwang University, Iksan, Republic of Korea*
[2]*Department of Dental Biomaterials and the institute of Biomaterials and Implants, Wonkwang University College of Dentistry, Iksan, Republic of Korea*

In this study, we investigated the bone regeneration potential of nickel-titanium (NiTi) shape memory alloy (SMA) plates modified with anodized nickel-titanium oxide nanotubes (NiTi-O nanotubes, NTO), gold (Au) coating, and visible-light (600 nm) irradiation. Five groups were established: NiTi, NTO, and Au-NiTi-O (ANT) as controls, and light-irradiated NTO/600 and ANT/600 groups (600 nm, 10 min, 5.5 mW/cm^2). Circular calvarial defects (8 mm) were created in 6-week-old rats, and bone regeneration was assessed at 2 and 6 weeks using micro-computed tomography and histological analyses. At 2 weeks, the ANT and ANT/600 groups exhibited higher new bone volumes (3.381 ± 1.220 and 2.606 ± 1.721 mm^3, respectively), although the differences were not statistically significant (p>0.05). At 6 weeks, significant differences were observed between the groups; the ANT group demonstrated the highest bone volume, whereas the NTO group showed significantly lower bone formation. However, no statistically significant enhancement specifically attributable to visible-light irradiation was detected when comparing the irradiated groups with their non-irradiated counterparts. Histological findings revealed consistent new bone formation adjacent to the NiTi plates in all groups, suggesting that the low bone volume in the NTO group was likely due to mechanical instability and plate displacement rather than material cytotoxicity. The limited photostimulatory effect was attributed to the non-porous plate geometry and attenuation of 600 nm light through the soft tissue. Consequently, while the modified NiTi surfaces demonstrated favorable biocompatibility, future studies should focus on developing mechanically stable porous NiTi plates and optimizing the optical parameters to achieve effective photoactivation.

Keywords : NiTi shape memory alloy, Gold coating, Plasmonic photocatalysis, Visible light irradiation; bone regeneration.